Colloids and Surfaces A: Physicochem. Eng. Aspects 496 (2016) 39–51

Contents lists available at ScienceDirect

Colloids and Surfaces A: Physicochemical and Engineering Aspects

journal homepage: www.elsevier.com/locate/colsurfa

Advanced and delayed filling or emptying of pore entities by vapor sorption or liquid intrusion in simulated porous networks

Jorge Matadamas[a], Reyna Alférez[b], Raúl López[c], Graciela Román[a], Isaac Kornhauser[b], Fernando Rojas[b,*]

[a] Dpto. de Ing. Eléctrica, Universidad Autónoma Metropolitana-Iztapalapa, P.O. Box 55-534, México D.F. 09340, Mexico
[b] Dpto. de Química, Universidad Autónoma Metropolitana-Iztapalapa, P.O. Box 55-534, México D.F. 09340, Mexico
[c] Instituto de Física Aplicada CONICET, Universidad Nacional de San Luis, Ejército de Los Andes 950, San Luis D5700HHW, Argentina

HIGHLIGHTS

- Pore networks of variable connectivity are simulated.
- Prohibition of geometrical interferences between neighboring voids is observed.
- N_2 sorption isotherms and Hg intrusion–extrusion curves have been simulated.
- Advanced and delayed adsorption and delayed Hg penetration have been identified.
- Pores subjected to advanced or delayed phenomena have been distinctly marked.

GRAPHICAL ABSTRACT

Pore networks have been simulated in silico to perform N_2 sorption and Hg porosimetry in order to identify advanced or delayed filling processes occurring in pore entities.

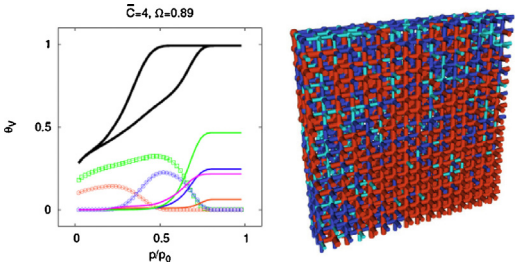

ARTICLE INFO

Article history:
Received 31 May 2015
Received in revised form
22 September 2015
Accepted 29 September 2015
Available online 24 October 2015

Dedicated to the memory of Prof. Vicente Mayagoitia, Pioneer in the description of advanced and delayed capillary phenomena.

Keywords:
Advanced adsorption
Delayed intrusion
Canthotaxis
DSBM approach
Variable connectivity pore networks

ABSTRACT

Recently, a combination of successive experimental sorption and intrusion processes, developed in the same porous material, has been found very useful to ascertain the mechanisms by which a specified fluid can fill or empty (cooperatively or not) the porous entities that constitute the substrate in question. Here, we have chosen porous substrates, modeled through the Dual Site-Bond Model, in order to simulate either sorption or intrusion–extrusion phenomena inside them. Afterwards, we have assessed the results obtained from these two techniques to describe the occurrence of cooperative phenomena during the filling or emptying of pore entities with a given fluid. The void entities involved in the development of irreversible phenomena (e.g. advanced adsorption, delayed intrusion, etc.) can be identified in each of these substrates in terms of their sizes and topology (i.e. the specific way by which these pores are interconnected to the other ones). The possible interrelation between assorted cooperative phenomena, taking place in the same porous adsorbent, is studied according to the type of porous material in hand.

* Corresponding author.
E-mail addresses: matahj@xanum.uam.mx (J. Matadamas), ralferez@xanum.uam.mx (R. Alférez), rlopez@unsl.edu.ar (R. López), grac@xanum.uam.mx (G. Román), jks@xanum.uam.mx (I. Kornhauser), fernando@xanum.uam.mx (F. Rojas).

http://dx.doi.org/10.1016/j.colsurfa.2015.09.072
0927-7757/

1. Introduction

1.1. Some advanced and delayed capillary phenomena occurring in porous media

The evolution of capillary processes in porous media is more often than not subjected to the irruption of diverse sorts of cooperative and obstructive phenomena [1–4]. In the case of capillary condensation and evaporation, processes such as advanced and delayed adsorption, as well as cavitation, and pore blocking are examples of those phenomena. The topology of the porous medium [5], i.e. the precise way by which void entities are distributed and interconnected to each other, greatly determine the outcome of such events. It is the objective of this contribution to discern which individual pore properties (e.g. geometry and size) and interconnection characteristics determine the existence or absence of the above cooperative and uncooperative processes in pore networks.

Let us think about a very simple example explaining both assisted (advanced) and delayed adsorption. First, let us explain what advanced and delayed adsorption mean. A pore entity of a given geometry and size in contact with a vapor phase can undergo capillary condensation. As the pressure is raised, a vapor-liquid phase transition eventually occurs and the whole void is filled with capillary condensate. However, when the pore is interconnected to a number of fellow cavities by narrower throats, it can happen that the filling of the cavity with condensate can only occur at a higher vapor pressure if compared to that employed to occupy the isolated (non-interconnected) cavity. This phenomenon is labeled as delayed adsorption. On the contrary, when a capillary is invaded by a liquid front proceeding from a neighboring cavity, it usually happens that the pressure required to fill this void with condensate, is lower if compared to the pressure needed to produce the vapor-liquid transition in the isolated pore. This last phenomenon is recognized as advanced adsorption. In order to have a clearer idea about what advanced and delayed capillary condensation stand for, let us start thinking about the conditions, i.e. relative pressure of the adsorptive, at which a site (spherical cavity) and a bond (cylindrical capillary) are filled with capillary condensate. The most immediate approximation for achieving this knowledge is to take the classical Kelvin equation [6] and, for simplicity, to just consider the capillary forces but not the surface forces arising from the pore walls. A second approximation to be included in the Kelvin expression is to assume that the condensate has the same properties as the bulk liquid. In this way, a spherical cavity of a given radius in order to be filled of condensate requires the relative pressure to be at least equal to the square root of the value assumed by this quantity when capillary condensation takes place inside a cylindrical pore of the same radius. In particular, let us now imagine a spherical cavity connected to four cylindrical capillaries (Fig. 1); this arrangement is now put in contact with a vapor phase. If the diameter of the spherical void is at least twice the size of the linked bonds, then,

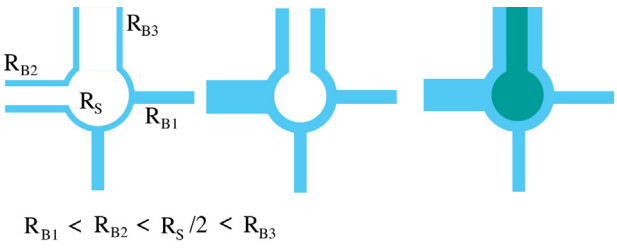

Fig. 1. For a site to be filled with condensate, at least *C-1* of its surrounding bonds have to be already filled with liquid. An empty bond, connected to an adjoining site that is being filled with condensate, will be invaded by liquid if the size sequence provided above is fulfilled. This phenomenon is known as advanced adsorption.

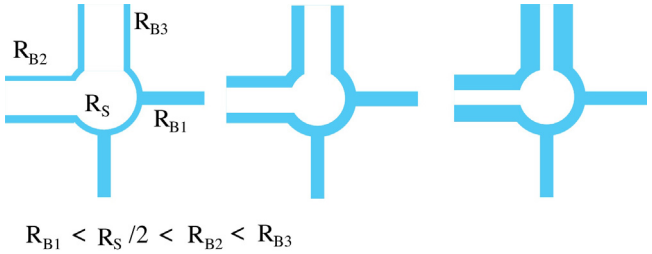

Fig. 2. A site is filled in a delayed fashion, since it is only occupied by condensate if a sufficient number of bonds has already been invaded with liquid.

according to the Kelvin equation, capillary condensation should firstly occur in these capillaries, beginning with the smallest and ending with the largest of these bonds. Subsequently, as the vapor pressure is further increased, the liquid-vapor *l-v* meniscus existing in the spherical site will be automatically displaced into the remaining empty bond until this last entity is entirely invaded by condensate. In contrast to this assisted filling of a cylindrical bond, in the case of the spherical cavity (Fig. 2), condensation is being delayed since it is required that either, all or all but one, of its surrounding bonds (not only one of them) are beforehand filled with condensate.

Given the right textural conditions of a given adsorbent, it may happen that an advanced filling of pore entities could be percolatively (i.e. intensively) extended to other zones of the porous medium in certain kinds of porous materials. The obstructive action of some fluid-containing pore entities, strategically located around certain positions of the pore structure, can effectively prevent the straightforward escape of a given fluid phase (usually liquid) contained in some parts of the porous network, this circumstance is labeled as the so-called pore-blocking effect. Additionally, this phenomenon, together with the cavitation process, is responsible of the steep aspect of the descending boundary curves depicted by many sorption isotherms.

With respect to liquid (e.g. mercury) intrusion in pore networks [7], a distinctive phenomenon is the canthotaxis effect. This delaying effect consists in the temporal anchoring of the advancing liquid-vapor meniscus at the entrance of a pore cavity, i.e. the zone at which an incoming bond is linked to a given site. The canthotaxis (cantho≡corner, edge; taxis≡to arrange or position at) process occurs due to the change in pore wall inclination as the advancing meniscus adapts its position from one wall to another, while the contact angle has to reestablish its value in passing from one solid wall to another. Canthotaxis is a phenomenon in itself, although there exists an interrelationship with the Dual Site-Bond Model (DSBM) approach (a general model of the porous network, developed in terms of sites and bonds, to be described in a later section). When the ratio between the diameters of a given site having an interconnected bond is high, a pronounced swelling of the liquid-vapor meniscus occurs at the interconnection perimeter existing between the site and bond until the pressure reaches a high enough value for penetrating into the cavity. When the ratio between the diameter of the site and its linked bond, is close to unity, then a less-pronounced swelling (and consequently a smaller pressure than in the other case) is required to intrude the site. In the case of liquid intrusion into pore networks, it can even surge the possibility of a very distinctive phenomenon: the kinetic energy of movement of liquid menisci can be transformed into an intrusion pressure that can penetrate narrow pores (i.e. in an advanced way) which, under static conditions, would be still uninvaded by the liquid phase.

A second effect that can take place during liquid extrusion is the snap-off of liquid threads inside tubular (bond) capillaries [7]. Due to this effect, portions of the intruded liquid can be left isolated from all liquid paths that lead to the outer surface of the intruded

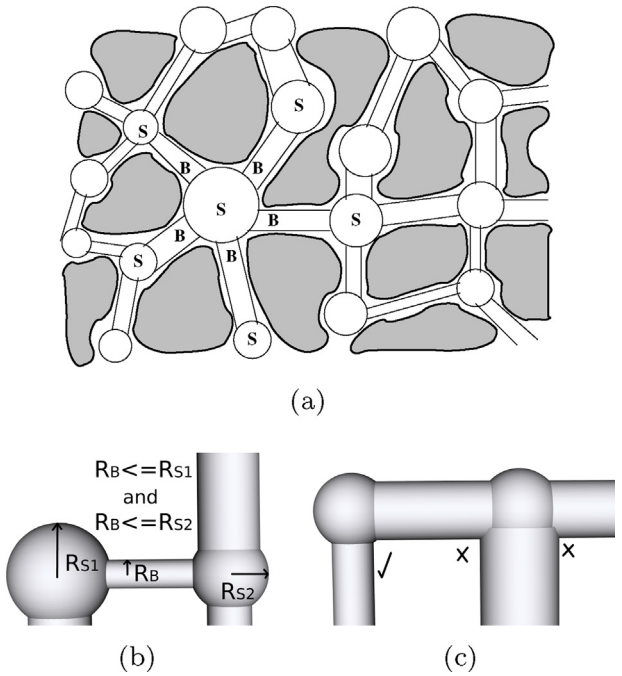

Fig. 3. (a) Schematic representation of sites (S) and bonds (B). (b) Graphic illustration of the Construction Principle (CP). (c) Geometric restrictions (GR) between neighboring bonds.

material. Islands of liquid can then remain trapped throughout the pore structure without no possibility of being extruded by simply decreasing the pressure exerted on this phase.

The modeling of adsorption–desorption and intrusion–extrusion processes in simulated pore networks, endowed with different textural characteristics, can shed light on upon the mechanisms by which the above phenomena proceed and also in the next important aspect: how the topology of the pore network brings about the possibility of observing advancing or delaying processes related to the development of capillary phenomena in porous substrates. Is it possible to design pore bodies in which cooperative advancing or obstructive (delaying) effects can be modulated to a desired extent?

Apparently, pores that are subjected to advanced adsorption are also responsible for the canthotaxis phenomenon when sites are exposed to liquid intrusion. On the same basis, cavities that are invaded with retard during capillary condensation are once more invaded likewise with liquid through intrusion. From the basic premises of the DSBM, it would be useful to know if the above assertions are right or not and also what would be the influence of the overlap between the site and bond size distribution on this matter. An additional parameter to take into account with respect to these facts could be the influence of the degree of connectivity of the void cavities with their neighbors.

2. Models and methods

2.1. The Dual Site-Bond Model

In this work, the DSBM [2,8–10] will be employed for the *in silico* simulation of pore networks. The fundamental basis of this model consists in grouping the void elements into two types (Fig. 3): the sites (chambers, cavities, antrae) and the bonds (necks, throats capillaries). For simplicity each site can be conceived as a hollow sphere of radius R_S; in turn, a bond can be imagined as a hollow cylinder of radius R_B. Each bond interconnects two sites in such a way that there exist C bonds linking each site with their fellow

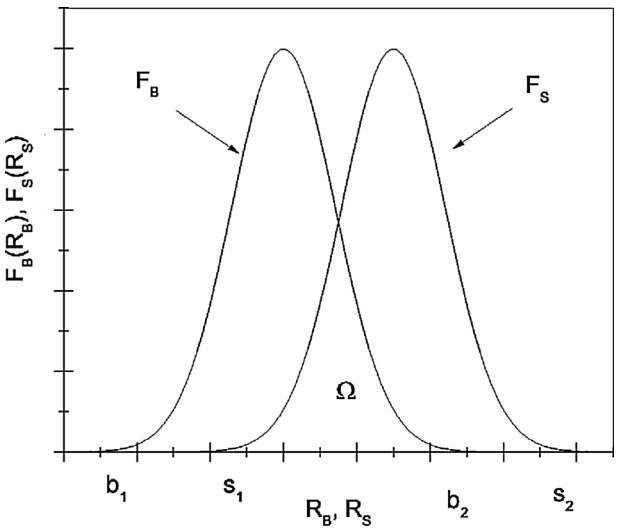

Fig. 4. Site- and bond-size distributions $F_S(R_S)$ and $F_B(R_B)$, respectively; b_1 corresponds to the size of the smallest bond, b_2 represents the size of the largest bond; in turn, s_1 is the size of the smallest site and s_2 depicts the size of the largest site. The overlap Ω is the common area shared by $F_S(R_S)$ and $F_B(R_B)$.

neighbors; C is called the connectivity of the site and this number can stay fixed or allowed to vary from site to site. Another fundamental aspect of the DSBM approach is to recognize that the size (i.e. diameter) of a given bond can never be larger but at most equal to the sizes of any of the two sites to which this capillary is linked (Fig. 3). This last statement is known as the Construction Principle (CP); this restriction can be adapted to additional requirements depending on the actual situation; for instance, the intersection of two neighboring bonds arriving to the same site can be prevented by an *ad hoc* CP as will be explained immediately below.

A very important aspect of physical networks, such as the pore arrangements that we are implementing herein, is the fact that two contiguous bonds (see Fig. 3) must not interfere with each other before converging into the site to which they are going to be attached. This kind of limiting situation is labeled as a geometric restriction (GR); of course, all pair of adjacent bonds must fulfill this stricter condition.

The corresponding CP when GR arise can be cited as follows: the size (i.e. diameter) of a given bond, besides of needing to be smaller or at most equal to the size of a site to which this capillary is linked, it must also be small enough as to prevent the existence of GR with all contiguous bonds that are surrounding the site. In the particular case of this work, we will be working with both the basic (no GR) and extended CP (GR prevention) visions in order to foresee the effect of each one of such restrictions on the topology of the pore network.

The overlap Ω between the site and bond size distributions (Fig. 4) is a fundamental parameter that determines the degree of size correlation existing among the void elements of the pore network. Pore networks simulated from size distributions overlapping a good deal are formed by extensive regions (i.e. homottatic domains [11]) in which the sizes of sites and bonds become very close to one another. In contrast, pore networks created from size distributions showing a null overlap between them consist of minute zones of sites and bonds of diverse diameters dispersed throughout the whole pore network.

Expressing the site size distribution as $F_S(R_S)$ and the bond size distribution as $F_B(R_B)$ Fig. 4, then the fraction of sites having sizes smaller than R is given by:

$$S(R) = \int_0^R F_S(R_S)dR_S \quad (1)$$

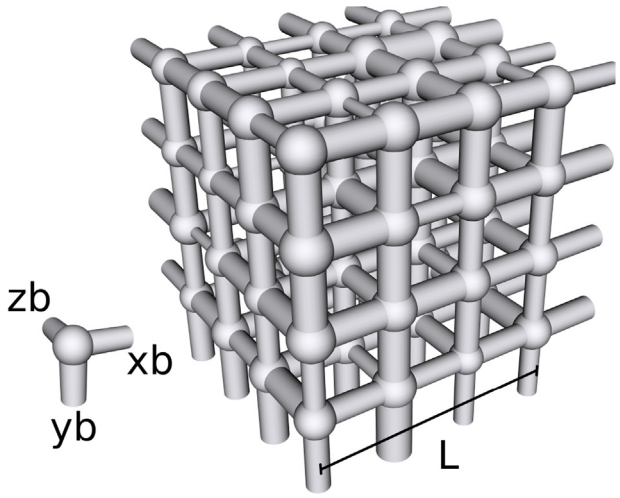

Fig. 5. Cubic Pore Network $L_S = 4$ and constant connectivity $C = 6$.

In turn, the probability to have a bond of size R or smaller is expressed as:

$$B(R) = \int_0^R F_B(R_B)dR_B \tag{2}$$

The CP gives rise to two autoconsistency laws in order to build valid (i.e. fulfilling the CP) pore networks. The first law guarantees that a sufficient amount of bonds of small sizes exists as to interconnect the sites arising from a given cavity size distribution. This law can be expressed as:

$$B(R) \geq S(R) \tag{3}$$

The second law guarantees that any bond of size larger than any site cannot be connected to the site in question. In order to enunciate this second law, it is first necessary to define the joint probability of having a bond of a given size R_B to be joined to a site of size R_S as:

$$F(R_S \cap R_B) = F_S(R_S)F_B(R_B)\varphi(R_S, R_B) \quad \forall R_S \geq R_B \tag{4}$$

The correlation function $\varphi(R_S, R_B)$ fulfils the following condition:

$$\varphi(R_S, R_B) = 0 \quad \forall R_S < R_B \tag{5}$$

2.2. In silico simulation of pore networks

The *in silico* representation of a pore network starts with the implementation of a given lattice; in this work, we have chosen a cubic arrangement ($C = 6$) for this task. A number $(N_S)^3$ sites together with $(3N_B)^3$ bonds are sorted out from their respective parent pore-size distributions (PSD); sites are allocated at the nodes of the lattice (Fig. 5). Bonds (in a proportion of 3:1, given the cubic geometry of the network) are linked to each site; however, the CP should be fulfilled every time a bond is connected to a site. An important concept for building a pore network is the notion of pore multiplex; in the case of our cubic geometry this arrangement consists in one site connected to three bonds, the other 3 bonds required to complete the total of six come from the interconnection of the site in question with three of its first neighboring sites

A more realistic representation of a pore network should consider more restrictions besides that considering that a site should be larger than any of the sizes of the bonds joined to it. For instance, one can consider that the connectivity is not constant throughout the arrangement; one site can adopt a maximum connectivity (e.g. six for a cubic network) and another one a minimum C (e.g. 0 for the case of a blind cavity). A second, and perhaps more important restriction, is that accounting for geometric restrictions as mentioned in a previous paragraph (Fig. 3).

One of the most resourced methods to simulate pore networks is based on a pure Monte Carlo Procedure [9]. This approach consists in assigning the sizes of all sites and bonds in a haphazard manner; obviously, when connecting pore elements this way multiple CP violations are involved thus rendering an invalid pore network arrangement. To overcome this situation, an intense pore-exchanging process has to be followed. One site at a given location is chosen at random and attempted to be exchanged with another site selected at another location; if the exchange causes that the number of CP violations to decrease or to remain the same, the swapping is accepted otherwise it is rejected. For the case of a cubic network, after one possible site exchange successful or not) three bond exchanges have to be attempted in order to fulfill the connectivity requirement. Notice has to be taken into account with respect to Ω, since valid interconnections result more difficult to carry out as this parameter becomes higher.

The approach previously described is a sequential method and for the construction of relatively small pore networks with a high overlap ($L_S = 64$, $\Omega \sim 1$) it takes a total processing time of the order of days, in a lone PC processor. Recently, a greedy sequential algorithm [12] was implemented to decrease the construction time of pore networks. In this method, several valid (i.e. respecting the pertinent CP) pore subnetworks are constructed separately and allocated at different positions in the lattice. In the end, the subnetworks are brought together, filling all possible gaps between them (while obeying, of course, the CP). This network is further subjected to a great number of Monte Carlo size exchanging attempts until a valid and anisotropic pore network is achieved.

In a more recent work [13], pore networks were built but now introducing GR (Fig. 3) by employing a multicore processor and a programming model involving an Open MP shared memory.

1. In order to simulate 3-D networks, the CP will be either considered in its simplest (i.e. no GR allowed) or in its extended formulation (i.e. GR considered). In our case, we have chosen to construct cubic networks ($C = 6$ or less because of the possibility of considering a variable connectivity).
2. Variable connectivity will be introduced via a fraction of bonds having a diameter equal to zero (i.e. these bonds are virtual since actually they are not existing). This artifice will allow us to vary connectivity from a maximum value ($C = 6$ for the case of a cubic network) to a minimum one of zero (i.e. all surrounding bonds being virtual). In the present manuscript, we will be dealing with two mean connectivity values: $C = 6$ and $\overline{C} = 4.2$; this last value is obtained when a fraction $f_0 = 0.3$ of virtual bonds (i.e. bonds having a radius equal to zero) is assumed to be repartitioned among the sites of the pore network [14]. Of course that the connection of one of these virtual bonds to sites is allowed under all circumstances; however, the presence of real bonds (those having a non zero radius) is what in reality determines the actual connectivity of each site.
3. The size of our simulated pore networks will be chosen as $L_S = 48$. This value has been selected since the RAM memory of our CPU processors is just enough for building networks of this size. This allowance is also influenced by the computing algorithm that is being used (i.e. recursive or not) since the subsequent simulation of capillary processes inside the *in silico* pore networks, usually requires of this recursivity (i.e. the state, empty or filled

with a given fluid, of a specific pore depends on the states of its neighboring pore elements).

2.3. Assessment and visualization of capillary processes inside the voids of simulated pore networks

The development of capillary phenomena in porous media can be described by mathematical models adapted from experimental observations that consider both physicochemical (temperature, pressure, surface tension, molar volume, etc.) as well as textural (pore shape, pore size, connectivity, surface area, etc.) parameters. In this work, we will be modeling sorption and intrusion/retraction phenomena as representative of typical capillary processes that take place in porous media. In this section, we will also include the visualization of simulated pore networks (in terms of the relative size and positioning of sites and bonds at distinct locations over assorted planes of a cubic lattice (the sites, idealized as spherical voids, will be allocated at the nodes of the lattice and the bonds will be cylindrical capillaries joining neighboring sites; a number of bonds (i.e. the connectivity *C*) will be surrounding and interconnecting each site; all pores will be drawn to a scale directly proportional to their sizes); likewise, the distribution of fluids (liquid, vapor) can be also visualized in terms of the occupied, with one fluid or another, sites or bonds.

2.4. N_2 sorption at 77K

The adsorption and capillary condensation processes are assumed to occur at constant temperature and are due to the conjoint action of the vapor pressure (p) and the capillary forces [14–17]. The adsorption process starts when an adsorbed layer of thickness t is developed on the surface (i.e. pore walls of sites and bonds) of the solid substrate. At a critical pressure (p_c) the capillary forces overcome the adhesion ones and the pore entity is completely filled with condensate. Importantly, during capillary condensation, not only the intrinsic geometric properties of a given pore entity but also the topology of the network determine the onset and outcome of the sorption process in question. This last statement implies that the present condition (filled with a given fluid) of the neighboring pore entities strongly influences the mechanism and extent of the capillary process under study. Capillary evaporation is the inverse process of capillary condensation; in this case, it is not only necessary that the pore entity (of a given geometry) has a size larger than a critical size (i.e. a value associated for instance to a critical pressure p_c) but also that a continuous vapor path can be established from the alluded pore to the outer vapor phase.

2.4.1. Computer algorithm for the simulation of N_2 sorption

In the case of capillary condensation, it is pertinent to define a critical condensation radius (R_c), which is increased proportionally to the rise of the vapor pressure (p) thus causing that inside the smallest pores can first happen the condensation of the surrounding vapor and then sequentually followed by the larger voids. Therefore, for a given R_c value, the cylindrical and spherical pores of radii $R <= R_c$ can be filled with condensate according to any one of the following mechanisms:

Condensation inside a cylindrical (bond) pore of radius R_B [18]:

a) The pore is filled on its own (i.e. the critical cylindrical meniscus formed on the pore walls is destabilized when $R_B \leq R_c/2$)
b) The capillary is filled assistedly through either one of the two sites connected to it if only $R_c/2 < R_B \leq R_c$ and, additionally, if one of the two sites linked to the bond is being filled with condensate.

Condensation inside a spherical (site) pore of radius R_S:

a) The filling of the pore is considered as normal (i.e. not delayed), if after the formation of a hemispherical meniscus on the surface of the site, the following conditions are also fulfilled: $R_S \leq R_c/2$ or $R_c/2 \leq R_S \leq R_c$ and at least *C-1* of its surrounding bonds are already filled with condensate.
b) The capillary condensation inside the site is delayed because of the existence of an incomplete (non continuous) hemispherical meniscus. The inherent reason of this delay, is that besides that the site must comply with the right size, i.e. if $R_c/2 \leq R_S \leq R_c$ it should also wait (in terms of relative pressure) until all *C* or at least *C-1* of its bonds are already filled with condensate (i.e. in the case of *C-1* bonds the remaining bond can be still empty). In this last case, the thickness of the adsorbed layer is kept equal to t_c, until the required number of *C-1* filled bonds is achieved and the site in question, together with the unfilled bond, are being filled with condensate.

The thickness of the adsorbed layer on the walls of void elements can be approximated from the following Harkins–Jura (HJ) equation; in fact, this equation is for valid flat surfaces, more exact expressions for calculating the thickness of the adsorbed layer in sites and bonds arise when taking into account the curvature of the pore walls.

$$t = \left(\frac{13.99}{0.0134 - \log \frac{p}{p^0}} \right)^{1/2} \tag{6}$$

During capillary evaporation, R_c, the critical radius of curvature (i.e. the radius of the *l-v* meniscus required for the pore to be emptied of condensate) is constantly decreaseing with p/p^0 in such a way that, in the absence of pore blocking effects, the larger pores would become the first to be emptied of liquid. Therefore, the following two conditions should be met in order for a given void to be empty of condensate: (i) $R \geq R_C$; and (ii) there should exist a continuous vapor path from the void in question to the outer vapor bulk phase. If the two above conditions are fulfilled concurrently, we could say that the pore is emptied of condensate *on schedule* (on time); however, if condition (i) is met whilst condition (ii) is not (at least for the moment), the pore is unable to evaporate its condensate and we could label it as a temporarily *blocked pore*.

2.5. Hg intrusion and retraction

Hg intrusion in pores takes place when the liquid phase is being pressurized. In the case of the cubic networks simulated in this work, the first void elements to be filled with mercury are the outer bonds at the periphery of the pore lattice, if only these entities comply with the right size, i.e.: $R \geq R_C$. This means that the current intrusion pressure, P_C, is linked to R_C, the actual critical radius of curvature required to occupy with the invading liquid a cylindrical bond of radius R, via the Washburn [19] equation.

$$P_C = 2\sigma^{lv} \cos\theta / R_C \tag{7}$$

σ^{lv} is the surface tension at the *l-v* interphase, and θ is the contact angle at the three-phase line of contact. Nevertheless, the intrusion of mercury inside a conical void, in which the pore walls have an inclination with respect to the pore axis, an advancing *l-v* meniscus of radius R is intruded according to the Cebeci [20] equation:

$$P^l = -\frac{2\sigma^{lv} \cos\Phi}{R \sin\beta} \tag{8}$$

where Φ is an angle that takes into account both the contact angle θ and α the inclination of the pore wall; i.e. $\Phi = \theta + \alpha$. In turn, β

Table 1
Structural properties of simulated 48 × 48 × 48 Pore Networks. D_{MS} is the mean site diameter size, D_{MB} is the mean bond diameter size, σ is the standard deviation (assumed the same for sites and bonds), Ω is the overlap and $\overline{C}$ the mean connectivity of the pore network.

Network	D_{MS}/nm	D_{MB}/nm	σ/nm	Ω	$\overline{C}$
4-1	9.2	4.0	0.4	0.00	4.2
4-2	4.8	4.0	0.4	0.61	4.2
4-3	4.2	4.0	0.4	0.90	4.2
4-GR	5.6	4.0	0.4	0.31	4.2
6-1	9.2	4.0	0.4	0.00	6
6-2	4.8	4.0	0.4	0.61	6
6-3	4.2	4.0	0.4	0.90	6
6-GR	6.4	4.0	0.4	0.13	6

is a complementary angle given by $\beta = \Phi - \pi$. This means that, for pores having pore wall inclination angles different than zero (with respect to the pore axis), the right equation to employ is the equation above.

Since the arrival and entrance of Hg to a site occurs through one of its delimiting bonds, the intrusion pressure would depend on the ratio between the size of the site and the size of the incoming bond, as will be expressed below.

With respect to the invasion of the inner voids of the network with Hg, the next premises arise:

(i) A bond of radius R_B is occupied with Hg when, besides of the requirement of existing a continuous liquid path from the Hg bulk phase to the pore in question, the pressure P^l becomes such that: $P^l = 2\sigma^{lv}\cos\theta/R_B$
(ii) The situation with the sites becomes rather different, since a special effect acknowledged as the canthotaxis phenomenon [7] arises at the bond-site joint. This event occurs when the *l*-*v* meniscus has to resume its contact angle, as the meniscus passes from one wall (cylindrical) to another (spherical). The *l*-*v* interface starts to swell until its curvature is such that the contact angle is reestablished with respect to the new wall. Depending on the ratio between the radius of the site and the radius of the bond, two equations arise in order to calculate the pressure required for the liquid phase to intrude the site. These equations are:

$$P^l = \begin{cases} \dfrac{2\sigma^{lv}}{R_{B,0}} & \text{if} R_{B,0} \le R_S|\cos\theta| \\ -\dfrac{2\sigma^{lv}}{R_{B,0}}\cos\left[\tan^{-1}\left(\dfrac{R_S^2}{R_{B,0}^2}-1\right)^{0.5}+\theta\right] & \text{if} R_{B,0} > R_S|\cos\theta| \end{cases}$$

Snap-off mechanism. In this case, a mercury thread is broken inside a capillary (bond) when the two following conditions are fulfilled [7]:

(i) The bond should have a radius R_B smaller than a certain R_{SO} threshold value (i.e. only the smaller bonds can be liable to snap-off), and
(ii) A residual Hg droplet existing in the bond is first straighten by adopting a thread-like shape and then eventually being broken due to the pulling action toward the Hg bulk phase of two continuous liquid paths existing at both ends of the capillary

Piston-like mechanism. The current retraction pressure P_C is related to a critical radius of curvature R_C, through the Washburn equation [19]. Two main cases arise:

- A site of size R_S containing mercury can be emptied of this liquid when the following triplet of conditions are fulfilled: (i) $R_S < R_C$, (ii) at least one of its C bonds is empty of liquid, and (iii) there

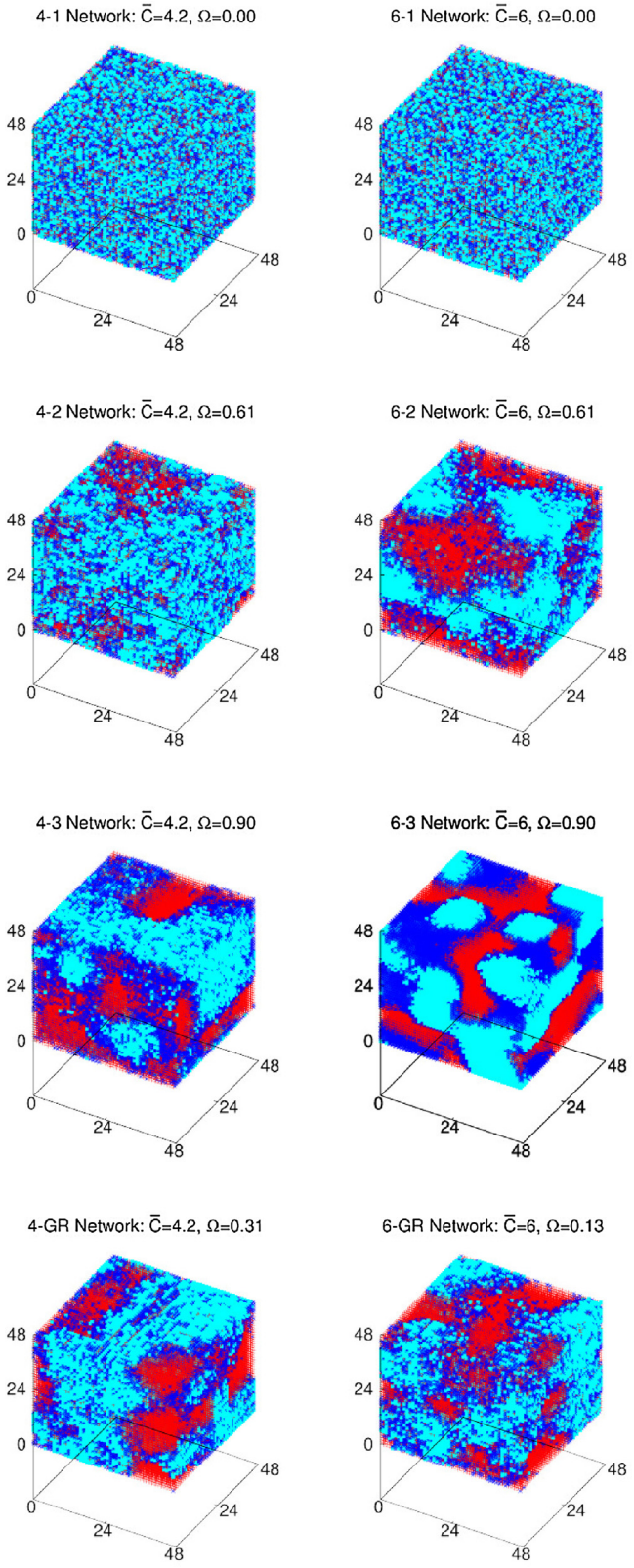

Fig. 6. Topology of simulated pore networks ($L_S = 48$). The red color indicates large pores sites, the blue color depicts medium size sites, and the cyan color represents small pores. The mean connectivity, the overlap between site and bond size distributions and existence of GR constraints appear as labels at the top edge of each figure. (For interpretation of the references to color in this figure legend, the reader is referred to the web version of this article.)

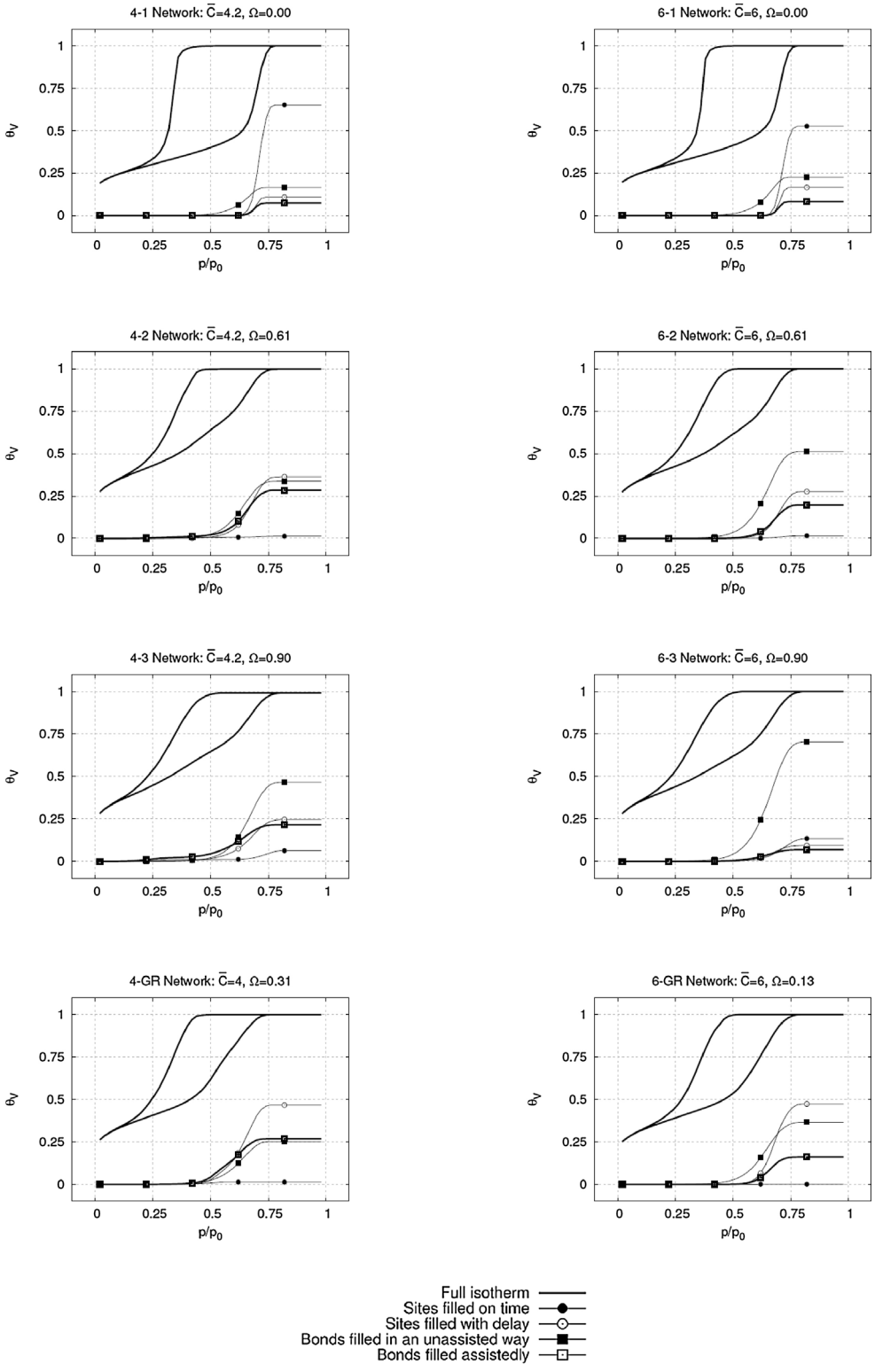

Fig. 7. N_2 sorption isotherms at 77K of simulated pore networks. The total isotherm is depicted with a black line; the associated isotherms are drawn as follows: bonds filled assistedly (full squares); bonds filled unassistedly (hollow squares); sites filled with delay (hollow circles); sites filled on time (filled circles).

exists a continuous liquid path from the site under analysis to the external bulk phase through at least one of its delimiting bonds.

- A bond of size R_B is going to be emptied of Hg if: (i) $R_B \leq R_C$, (ii) at least one of its two delimiting sites is empty, and (iii) there exists a continuous liquid path from one end the bond in question to the outer Hg bulk phase.

3. Results and discussion

3.1. Topology of pore networks

The pore networks were simulated *in silico* by means of a PC computer with an Intel Core i7-4770 Quad-Core processor running at @ 3.40 GHz and endowed with 16 Gb of RAM. Each pore network

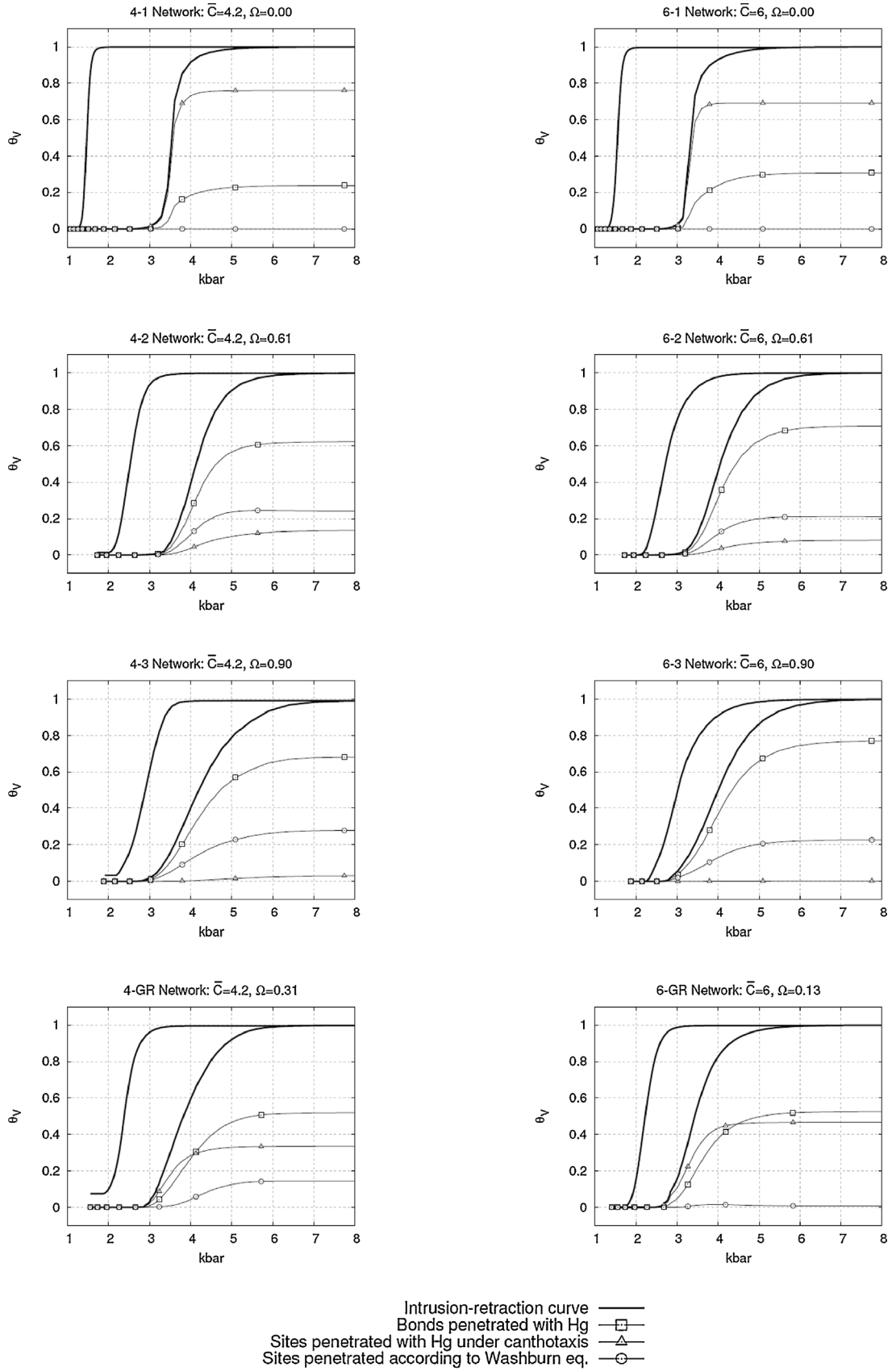

Fig. 8. Hg intrusion–extrusion isotherm curves obtained from simulated pore networks. θ_v is the fraction of the pore volume occupied with Hg. The labels appearing at the top of each graph display the mean connectivity, overlap and GR occurrence or not.

consists of a cubic lattice containing $48 \times 48 \times 48$ sites and their corresponding $3 \times 48 \times 48 \times 48$ bonds.

Table 1 lists the values of the Gaussian site and bond distribution curves together with the overlap Ω and mean connectivity C of each of the pore networks that have been employed in this work. Two main kinds of pore networks were built: (i) networks with constant connectivity, $C = 6$, subjected or not to GR; (ii) networks with variable connectivity $\overline{C} = 4.2$, including GR or not. D_{MS} is the site distribution mean size; D_{MB} is the bond distribution mean size; σ is the standard deviation (assumed the same for both sites and bonds); Ω is the overlap between size distributions; $\overline{C}$ is the mean connectivity.

The topology of the simulated pore networks can be displayed in terms of the allocation of large, medium, and small pore entities. To do this, the site size distribution has been subdivided in three regions, equivalent to the same area; the first zone corresponds to small pore entities, the second zone to medium size pores, and the last zone to large void entities. Fig. 6 shows the topology of each network. Even if the images in this last figure are obtained for sites, it is expected that the same kind of topology would be applicable to the bond entities.

In Fig. 6 the following characteristics are evident:

- The overlap Ω between the site and bond-size distributions promotes the segregation of the pore network into zones of small, medium and large pore entities. The medium size sites are intercalated between the small and large cavities of the network. This effect is more marked for $C = 6$ than for $\overline{C} = 4.2$.
- As expected, when $\Omega = 0$ pores are allocated *ad libitum* (randomly) throughout the network, especially when GR are absent but not quite as GR are present.
- The existence of GR between neighboring bonds converging to a site causes a kind of desegregation of the three pore size zones. This could mean that rather than creating regions of big, medium and small void elements, the pore cavities share bonds that can be connected to neighboring sites in a way that these bonds will not be interfere with each other. This kind of re-accommodation could be viewed as a compensation effect against segregation of pore sizes.

3.2. N_2 sorption

The simulated N_2 sorption isotherms at 77 K on the pore networks modeled *in silico* were calculated in terms of the repartition of the different kinds of fluids inside the void elements. The diverse contributions to the total adsorbed amount can be visualized in the following way (see Fig. 7):

The total isotherm is depicted in black; associated isotherms are drawn as follows: bonds filled assistedly (black-filled squares); bonds filled unassistedly (hollow squares); sites filled with delay (hollow circles); sites filled on schedule (i.e. with no delay) (black-filled circles).

- Empty sites containing an adsorbed layer of thickness t_S. These are cavities having an adsorbed layer and in which the complete filling of the site by capillary condensation has not yet taken place.
- Empty bonds holding an adsorbed layer of thickness t_B. These are capillaries with an adsorbed layer; capillary condensation or advanced adsorption by liquid displacement has not yet occurred in this entity.
- Sites filled on schedule. These are pores in which all their surrounding bonds have already been filled with condensate and the vapor pressure is high enough as to provoke the vapor–liquid phase transition to occur inside the cavity.

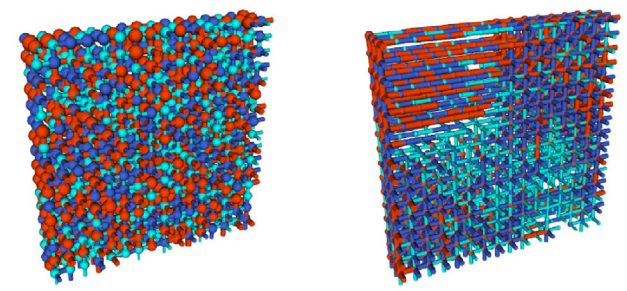

(a) Network Topology: Big (red), medium (blue), and small (cyan) pore entities.

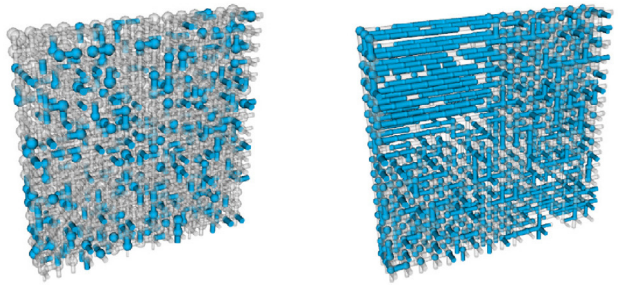

(b) Capillary condensation: In blue color sites filled with delay and bonds filled in advance. Gray elements sites and bonds filled on schedule.

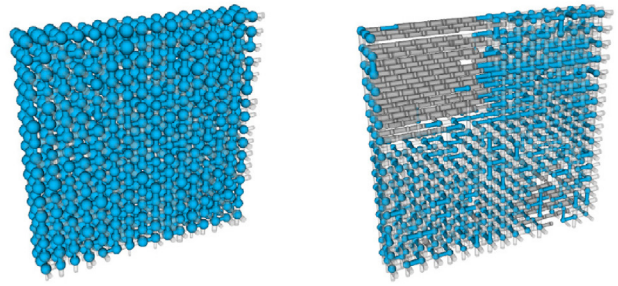

(c) Hg intrusion: In blue sites and bonds participating in the canthotaxis phenomenon. In gray pore elements that are penetrated under no canthotaxis.

Fig. 9. Pore Networks 4-1 (left) and 4-GR (right). Topology (top) and recognition (middle and bottom) of assisted filling of pore entities during sorption and Hg intrusion–extrusion processes. (a) Network Topology: Big (red), medium (blue), and small (cyan) pore entities. (b) Capillary condensation: In blue color sites filled with delay and bonds filled in advance. Gray elements sites and bonds filled on schedule. (c) Hg intrusion: In blue sites and bonds participating in the canthotaxis phenomenon. In gray pore elements that are penetrated under no canthotaxis. (For interpretation of the references to color in this figure legend, the reader is referred to the web version of this article.)

- Sites filled with delay. In this case, sites have an incomplete set of delimiting bonds already filled with condensate and still require vapor condensation to take place in one or more bonds. When the last (i.e. the largest) of these bonds is occupied by condensate, the site (together with its still unfilled bonds) is immediately filled with liquid.
- Bonds filled on time. These pores are filled according to the Kelvin or BdB equation [21], independently of the state (filled or empty of condensate) of their neighboring entities.
- Bonds filled in advance. These are capillaries that are filled from a liquid front that proceeds from one of their connected sites as these pores are occupied by condensate. This advanced filling can

be spread to pore entities connected to the bond in question or even beyond of them.

The following observations can be inferred from the aspects of the sorption isotherms:

- The amount of bonds filled in advance (assisted filling) due to the liquid flow created from a delimiting site becomes more and more appreciable as Ω increases;
- In the same sense, consideration of GR also contributes to a significant rise in the number of bonds filled in an assisted manner by liquid flow incoming from a contiguous site;
- Sites filling on schedule (i.e. those that fill with condensate once all their surrounding bonds are occupied with it) correspond almost exclusively to networks for which Ω = 0;

Fig. 8 shows the Hg intrusion-extrusion isotherm curves obtained from simulated pore networks. The label at the top of each graph depicts the mean connectivity, overlap and the consideration or not of GR.

Hg intrusion of sites takes place after the *l-v* meniscus is subjected to canthotaxis at the site-bond interconnection. The intensity of this last phenomenon is greater in pore networks of low overlap (Ω = 0) while an important contribution is also present in networks subjected to GR. Additionally, as Ω increases the canthotaxis effect becomes of a lesser degree. The number of bonds penetrated according to the classical Washburn equation is only important when Ω attains relatively high values. This last assertion implies that the use of the Washburn equation to calculate pore size values from intrusion experiments can be subjected to a good deal of uncertainty. Another point that deserves attention is that Hg incomplete extrusion has something to see with GR presence; it seems that bonds participating of this effect can be associated to Hg snap-off. Likewise, structures having a low Ω are practically free of snap-off occurrence. For networks undergoing GR limitations, most bonds are penetrated after suffering of canthotaxis, in contrast with bonds that form part of networks displaying either low or high Ω, in the absence of GR.

3.3. *Evaluation of the extent of advanced and delayed filling or emptying of pore entities*

An important aspect with respect to the calculation of N_2 sorption isotherms is linked to the comparison between PSDs calculated from the simulated sorption curves and the precursory site- and bond-size distributions. This assessment can contribute to the identification and evaluation of the extent of advanced or delayed phenomena occurring in the pore entities during the capillary process that is taking place. For instance, if at a certain pore size the PSD obtained from the simulated desorption isotherm lies above the parent PSD curve, this could mean that an advanced adsorption phenomenon is taking place in the pore sizes under analysis. On the other hand, if the PSD obtained from the adsorption boundary curve is located below the precursory PSD curve, then it is expected that a delayed filling of pore cavities is arising. Therefore, a complete overlap between calculated and precursory PSD curves is, in most cases, improbable to happen because of the presence of advanced or delayed phenomena. The comparison between the PSDs have been accomplished by transforming the amount adsorbed inside the simulated pore networks in terms of millimoles (or cm^3 STP) of N_2 per gram of adsorbent. The adsorbent mass is calculated by assuming a silica substrate (density equal to 2.2 g/cm^3); the corresponding adsorbent volume is obtained by subtracting the total void volume (sites + bonds) from the total volume (voids + solid, i.e. corresponding to the volume of the cubic lattice). With respect to Hg porosimetry, we have obtained the respective

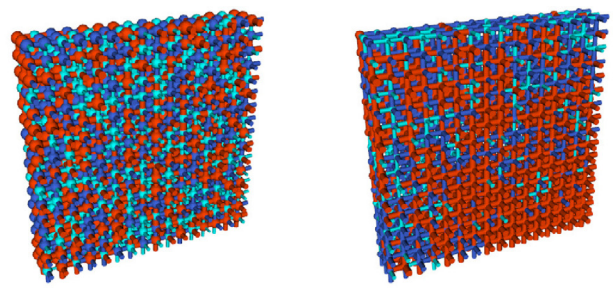

(a) Network Topology: Big (red), medium (blue), and small (cyan) pore entities.

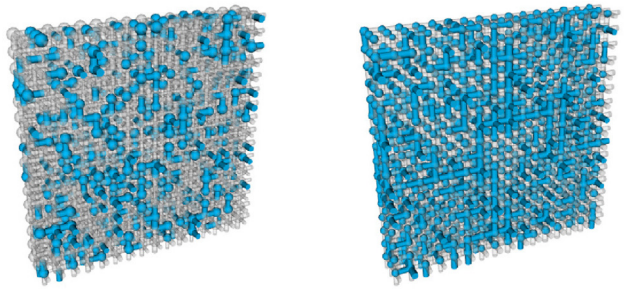

(b) Capillary condensation: In blue color sites filled with delay and bonds filled in advance. Gray elements sites and bonds filled on schedule.

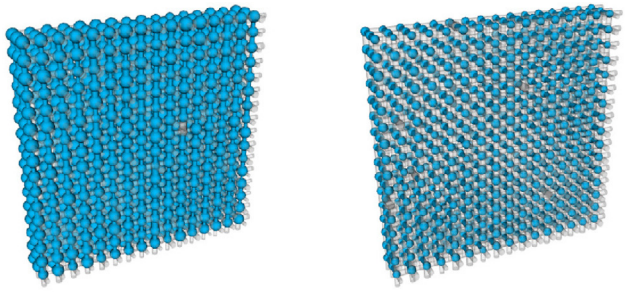

(c) Hg intrusion: In blue sites and bonds participating in the canthotaxis phenomenon. In gray pore elements that are penetrated under no canthotaxis.

Fig. 10. Pore Networks 6-1 (left) and 6-GR (right). Topology (top) and recognition (middle and bottom) of assisted filling of pore entities during sorption and Hg intrusion-extrusion processes. (a) Network Topology: Big (red), medium (blue), and small (cyan) pore entities. (b) Capillary condensation: In blue color sites filled with delay and bonds filled in advance. Gray elements sites and bonds filled on schedule. (c) Hg intrusion: In blue sites and bonds participating in the canthotaxis phenomenon. In gray pore elements that are penetrated under no canthotaxis. (For interpretation of the references to color in this figure legend, the reader is referred to the web version of this article.)

intrusion-extrusion curves (Fig. 8) in terms of the volume intruded as function of the penetration pressure.

In our simulated pore networks, as it will be shown below, we have identified the way by which interconnected sites and bonds have been filled with capillary condensate. The pore entities (either sites or bonds) that have been filled with condensate in an assisted manner or intruded with Hg after canthotaxis have been marked in blue in some slices of the pore networks, Figs. 9 and 10, which show the appearances of lowly correlated (4.1 and 6.1 Networks) contrasted against the aspects depicted by highly correlated (4-GR and 6-GR Networks) substrates. In turn, those pore elements that have

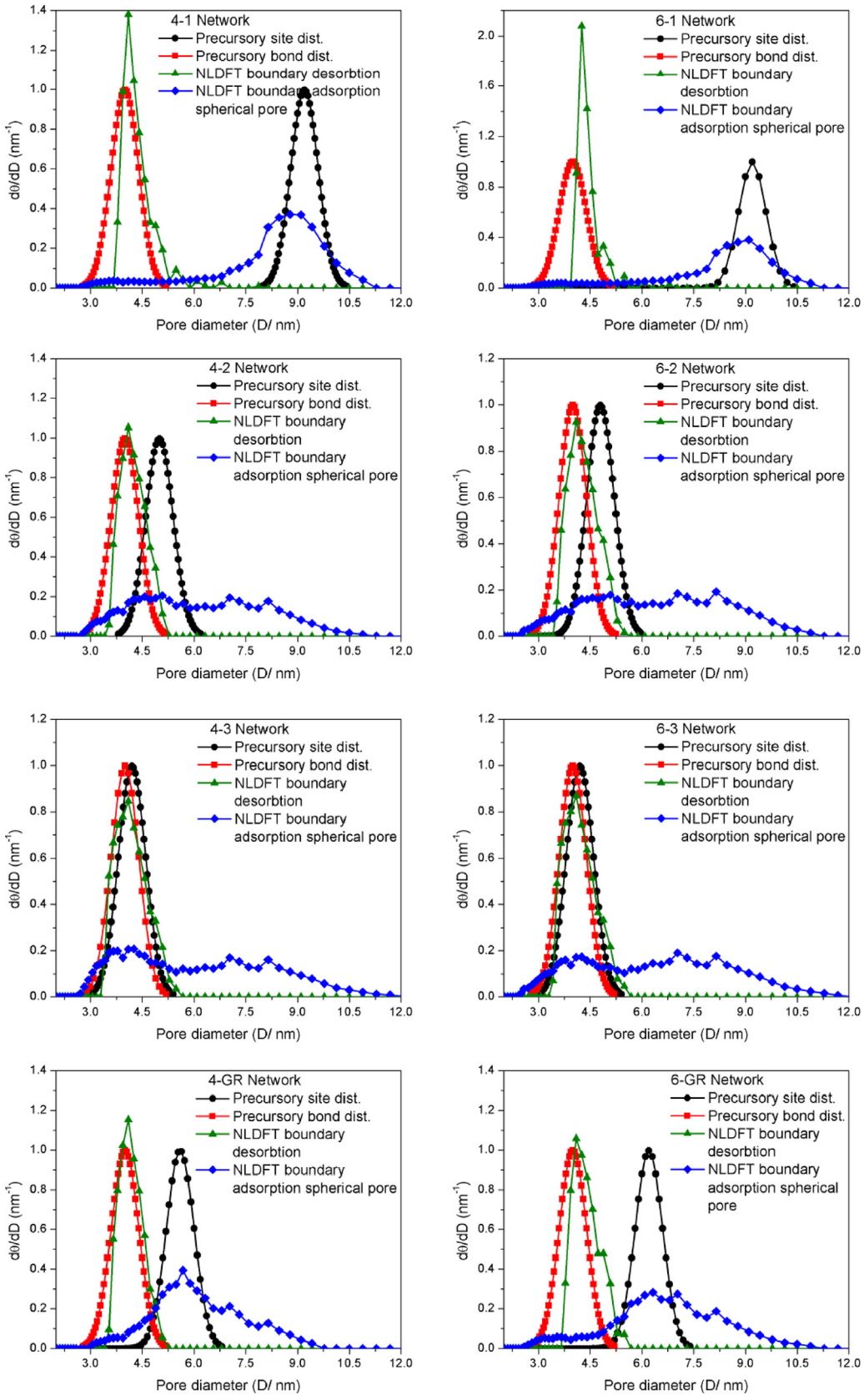

Fig. 11. Comparison between pore-size distributions calculated from simulated pore networks and precursory site and bond distributions. The calculation kernels are shown in the figures inset.

been filled with condensate unassistedly or under no canthotaxis have been labeled with gray-filled symbols.

The PSD curves have been obtained from application of the NLDFT treatment [22] to the boundary adsorption and boundary desorption N_2 isotherms. The shape of bonds has been chosen as cylindrical while sites have been assumed as spherical cavities. The particularities of the PSD curves illustrated in Fig. 11 can be described as follows:

Sample 4-1. The PSD calculated from the boundary desorption isotherm is recovered a good deal in relation to the precursory bond distribution. Likewise, although in a lesser extent, the PSD obtained from the adsorption boundary isotherm (assuming spherical pores) looks fairly similar to the precursory site distribution. All this means that in this sample, corresponding to $\Omega = 0$, first bonds and then sites are filled independently and consecutively; perhaps some delayed adsorption of sites is occurring, this being the reason why the precursory PSD lies above the calculated PSD from the adsorption boundary curve.

Sample 6-1. Something similar to what occurs in sample 4-1 is taking place in this substrate. Sites fill once their surrounding bonds are filled with capillary condensate. A good fit, between the initial and calculated PSDs from the desorption boundary curve, is observed for this sample, which depicts a null overlap between the site and bond size distributions. The agreement between the PSD obtained from the adsorption isotherm and the precursory site size distribution is not complete but it is proximate enough.

Samples 4-2 and 6-2. When Ω starts arising, the PSD calculated from the adsorption boundary isotherm is markedly different from the original (precursory) site PSD. However, the agreement between the precursory bond PSD and that calculated from the desorption boundary isotherm, continues to be very close. It seems that the delayed filling of sites is taking place in a more important extent. Here, it would be convenient to contrast these PSD curves with the PSD obtained from mercury intrusion in order to further certify the last observation.

Samples 4-GR and 6-GR. Fairly good agreements are obtained between the precursory bond size distribution and the PSD proceeding from the desorption isotherm. In turn, the PSD arising from the adsorption boundary isotherm overlaps fairly but partially with the precursory site-size distribution. This is evidence of the existence of some delayed filling of sites since the calculated pore diameter values range within largers if compared to those existing in the parent site distribution. In turn, bonds appear to be mostly filled on schedule (i.e. advance adsorption of these elements is taking place to a limited extent).

Again, the topology (in terms of the distribution of pore sizes over assorted planes of the cubic pore network) can be appreciated in Figs. 9 and 10; additionally the PSD curves obtained from the analysis of the N_2 sorption isotherms are shown in Fig. 11. Nevertheless, the most striking evidence, concerning the pore entities that are filled with capillary condensate in a cooperative or uncooperative way, has been identified in Figs. 9 and 10. In this case, sites filled with delay or bonds filled in advance have been labeled with blue-filled symbols, whilst sites or bonds filled unassistedly have been marked with gray-filled symbols. In the same figures, for Hg porosimetry, sites subjected to the canthotaxis phenomenon are labeled in blue while sites or bonds filled under no canthotaxis are marked with gray-filled symbols. Therefore, the extent of the assisted or unassisted sorption phenomena can be assessed from the aspects of pore sections depicted in Figs. 9 and 10.

The proportion of sites filled with delay, in contrast to those sites filled in time, can be appreciated from the appearance of Figs. 9 and 10. The amount of sites filled with delay is higher for pore networks showing low overlap (i.e. 6-1 and 4-1 networks); the pore arrangements allowing for GR (i.e. 4-GR and 6-GR networks) display a good

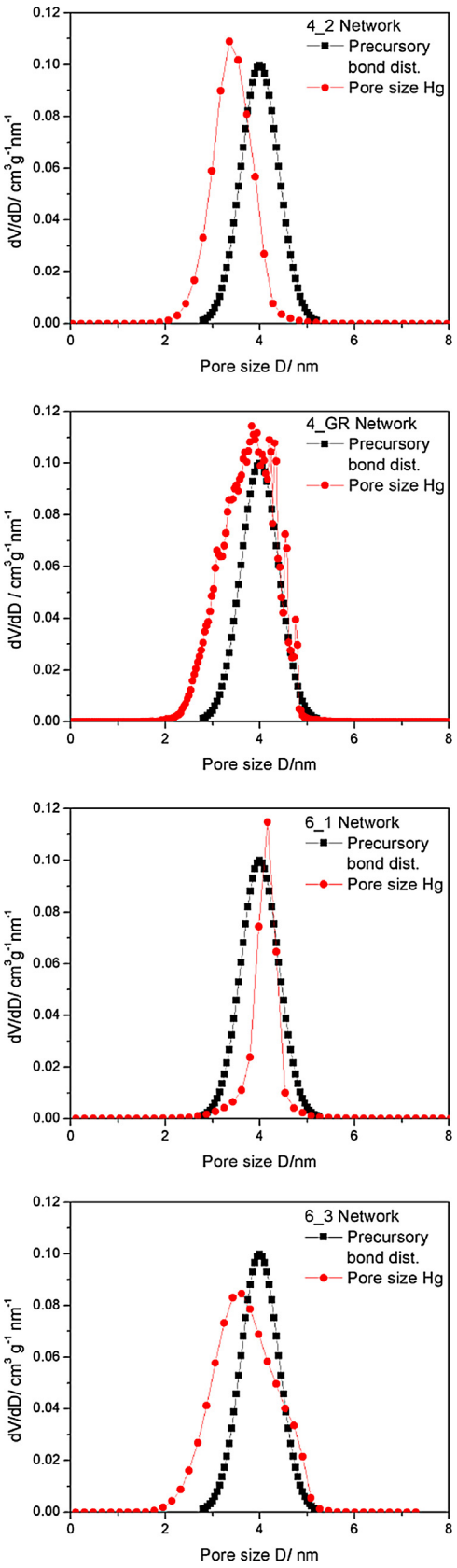

Fig. 12. Pore size distributions calculated from the Hg intrusion curves of samples 4_2, 4_GR, 6_1 and 6_3.

deal of pore entities that show, on the one hand, an advanced filling of bonds during sorption processes, and on the other hand, a delay for being penetrated with Hg during liquid intrusion.

One of the potential aims of this work is to employ the modeling approach described for recovering a more accurate PSD than traditional method do. For achieving this goal is important to consider the morphology and topology of the porous network under analysis. Specifically, in the present work, when performing the PSD calculation from Hg intrusion, the following results are found (see Fig. 12). The PSD's obtained from the analysis of Hg intrusion curves (for some assorted substrates) render a good agreement if compared to the precursory bond size distribution curves. Apparently, there is still no way to distinguish the sizes of the sites. The fitting of bond sizes between the precursory bond distribution and those calculated from the intrusion curve, becomes even better when the pore networks are subjected to GR. The inherent reason could be that canthotaxis is almost omnipresent in most pore networks; this happens because from the very definitions of sites and bonds, together with the CP, the access of the non-wetting liquid (Hg) into the sites is controlled by the latter phenomenon. When there arises a high Ω between the site and bond size distributions, it happens that when the bond-site entrance is overcome by the liquid–vapor meniscus, the passage into the inner cavities becomes percolative; this being the reason why a better agreement between the original bond size distribution and the PSD calculated for the 4-GR and 6-GR pore networks occurs.

4. Conclusions

Advanced or delayed processes with respect to the filling or emptying of pore entities during the development of capillary processes in porous media, are the rule rather than the exception. Depending on the type of pore structure, this being strongly associated to the overlap existing between the bond- and site-size distributions, results the intensity of the above mentioned cooperative phenomena. For pore networks exhibiting low overlap, while bonds are filled with condensate at low relative pressures, sites should wait until the required *l-v* meniscus is constructed along the perimeter of the cavity in question. On the other hand, Hg intrusion is subjected to intense canthotaxis at each pore mouth. As the overlap increases, and geometrical restrictions arise between neighboring bonds converging to site, the presence of cooperative phenomena is more and more prominent. Determination of pore-size distributions are very much affected by the irruption of delayed or advanced capillary processes; the interpretation of these results could be misleading if cooperative phenomena are not considered at all. Nowadays, methods employing hysteresis scanning curves or consecutive sorption-intrusion procedures on the same porous network can shed light into a more correct determination of pore structure parameters.

Acknowledgements

We thank the SEP-PRODEP Network Diseño Nanoscópico y Textural de Materiales Avanzados, Project Síntesis y Fisicoquímica de Materiales Mesoporosos (UAM-I CA-31 Fisicoquímica de Superficies). JM thanks the CONACyT for the scholarship support.

References

[1] I. Hitchcock, M. Lunel, S. Bakalis, R.S. Fletcher, E.M. Holt, S.P. Rigby, Improving sensitivity and accuracy of pore structural characterisation using scanning curves in integrated gas sorption and mercury porosimetry experiments, J. Colloid Interface Sci. 417 (2014) 88–99, http://dx.doi.org/10.1016/j.jcis.2013.11.025.
[2] J. Matadamas-Hernandez, G. Roman-Alonso, F. Rojas-Gonzalez, M. Castro-Garcia, A. Boukerche, M. Aguilar-Cornejo, S. Cordero-Sanchez, Parallel simulation of pore networks using multicore cpus, IEEE Trans. Comput. 63 (6) (2014) 1513–1525, http://dx.doi.org/10.1109/TC.2012.197.
[3] V. Mayagoitia, I. Kornhauser, Capillary processes in porous networks (2) capillary condensation and evaporation, in: Proceedings of the International Symposium on Principles and Application of Pore Structural Characterization, Arrowsmith, Bristol, 1883, pp. 27–35.
[4] V. Mayagoitia, F. Rojas, I. Kornhauser, Pore network interactions in ascending processes relative to capillary condensation, J. Chem. Soc., Faraday Trans. 1 (81) (1985) 2931–2940, http://dx.doi.org/10.1039/F19858102931.
[5] V. Mayagoitia, M. Javier Cruz, F. Rojas, Mechanistic studies of capillary processes in porous media. Part 1. Probabilistic description of porous media, J. Chem. Soc., Faraday Trans. 1 (85) (1989) 2071–2078, http://dx.doi.org/10.1039/F19898502071.
[6] S. Gregg, K. Sing, Adsorption, Surface Area, and Porosity, Academic Press, London, 1991.
[7] I. Kornhauser, C. Felipe, J. Esparza, A. Domínguez, F. Rojas, Mercury intrusion effects modelled in pores with axial symmetry and attenuated cross section, Adsorpt. Sci. Technol. 31 (2-3) (2013) 249–261, http://dx.doi.org/10.1260/0263-6174.31.2-3.249.
[8] V. Mayagoitia, F. Rojas, I. Kornhauser, H. Pérez-Aguilar, Modeling of porous media and surface structures: their true essence as networks, Langmuir 13 (5) (1997) 1327–1331, http://dx.doi.org/10.1021/la950812m.
[9] S. Cordero, F. Rojas, J.L. Riccardo, Simulation of three-dimensional porous networks, Colloids Surfaces A: Physicochem. Eng. Asp. 187-188 (2001) 425–438, http://dx.doi.org/10.1016/S0927-7757(01)00610-0.
[10] S. Cordero, I. Kornhauser, A. Domínguez, C. Felipe, J. Esparza, F. Rojas, R. López, A. Vidales, J. Riccardo, G. Zgrablich, Review site-bond network modeling of disordered porous media, Part. Part. Syst. Charact. 21 (2) (2004) 101–116, http://dx.doi.org/10.1002/ppsc.200400926.
[11] S. Ross, J. Olivier, On Physical Adsorption, John Wiley, New York, 1964.
[12] G. Román-Alonso, F. Rojas-González, M. Aguilar-Cornejo, S. Cordero-Sánchez, M. Castro-García, In-silico simulation of porous media: conception and development of a greedy algorithm, Microporous Mesoporous Mater. 137 (1-3) (2011) 18–31, http://dx.doi.org/10.1016/j.micromeso.2010.08.016.
[13] A. Gonzalez-Mendez, G. Roman-Alonso, F. Rojas-Gonzalez, M. Castro-Garcia, M. Aguilar-Cornejo, S. Cordero-Sanchez, Construction of porous networks subjected to geometric restrictions by using openmp, in: 2014 IEEE International Workshop on Parallel and Distributed Scientific and Engineering Computing (PDSEC'14), IEEE Computer Society, 2014.
[14] F. Rojas, I. Kornhauser, C. Felipe, J.M. Esparza, S. Cordero, A. Dominguez, J.L. Riccardo, Capillary condensation in heterogeneous mesoporous networks consisting of variable connectivity and pore-size correlation, Phys. Chem. Chem. Phys. 4 (2002) 2346–2355, http://dx.doi.org/10.1039/B108785A.
[15] V. Mayagoitia, F. Rojas, I. Kornhauser, Domain complexions in capillary condensation. Part 1. The ascending boundary curve, J. Chem. Soc., Faraday Trans. 1 (84) (1988) 785–799, http://dx.doi.org/10.1039/F19888400785.
[16] V. Mayagoitia, B. Gilot, F. Rojas, I. Kornhauser, Domain complexions in capillary condensation. Part 2. Descending boundary curve and scanning, J. Chem. Soc., Faraday Trans. 1 (84) (1988) 801–813, http://dx.doi.org/10.1039/F19888400801.
[17] M. Ponce, L. Munguía, M. Esparza, I. Kornhauser, F. Rojas, On scrutinizing the classical polanyi adsorption potential theory for vapour uptake occurring in the mesopores of curved shapes, Adsorpt. Sci. Technol. 29 (6) (2011) 585–594, http://dx.doi.org/10.1260/0263-6174.29.6.585.
[18] D. Everett, J. Haynes, Model studies of capillary condensation. I. Cylindrical pore model with zero contact angle, J. Colloid Interface Sci. 38 (1) (1972) 125–137, http://dx.doi.org/10.1016/0021-9797(72)90228-7.
[19] E.W. Washburn, The dynamics of capillary flow, Phys. Rev. 17 (1921) 273–283, http://dx.doi.org/10.1103/PhysRev.17.273.
[20] O.Z. Cebeci, The intrusion of conical and spherical pores in mercury intrusion porosimetry, J. Colloid Interface Sci. 78 (2) (1980) 383–388, http://dx.doi.org/10.1016/0021-9797(80)90577-9.
[21] J. Broekhoff, J. de Boer, Studies on pore systems in catalysts, J. Catal. 9 (1) (1967) 8–14.
[22] P.I. Ravikovitch, A.V. Neimark, Characterization of micro- and mesoporosity in SBA-15 materials from adsorption data by the NLDFT method, J. Phys. Chem. B 105 (29) (2001) 6817–6823, http://dx.doi.org/10.1021/jp010621u.